encit 2020

ABCM Associação Brasileira de Engenharia e Ciências Mecânicas

18th Brazilian Congress of Thermal Sciences and Engineering
November 16-20, 2020 (Online)

ENC-2020-0675
$CaCO_3$ INCRUSTATION IMPACT ON PRESSURE DROP IN SAND CONTROL SYSTEMS BY CFD TECHNIQUE

Ayrton Cavallini Zotelle
Lucas Spancini Bobbio
João Henrique Sartori Vieira
Renato do Nascimento Siqueira
Instituto Federal do Espírito Santo, Department of Mechanical Engineering, Rod. BR 101 North, km 58, São Mateus, Espírito Santo, 29932-540, Brazil.
ayrton.zotelle1@hotmail.com
lucas.bobbio@hotmail.com
joao.sartoriv@gmail.com
renatons@ifes.edu.br

André Campanharo Gabriel
Universidade Federal do Espírito Santo, Department Mechanical Engineering, Av. Fernando Ferrari, 514, Goiabeiras, Vitória, Espírito Santo, 29075-910, Brazil.
andrecampanharo@hotmail.com

Fábio de Assis Ressel Pereira
Universidade Federal do Espírito Santo, Department of Industrial Technology, Av. Fernando Ferrari, 514, Goiabeiras, Vitória, Espírito Santo, 29075-910, Brazil.
fabio.a.pereira@ufes.br

André Leibsohn Martins
Petrobras, Horácio Macedo street 950, Ilha do Fundão Cidade Universitária, 21941-915, Rio de Janeiro, Rio de Janeiro, Brazil.
aleibsohn@petrobras.com.br

Abstract. *During the secondary recovery process, due to the incompatibility between formation and injected water, precipitation of inorganic salts, as the calcium carbonate, can occur. The salt are usually cared with the flow and it can reach the well equipment, as the sand control screens. The deposition of the inorganic salt can reduce the flow area, increasing the pressure drop, or completely obstruct the fluid passage. Using correlations available in the literature and elaborating a sub routine, this paper model the influence of the calcium carbonate incrustations on the pressure drop in sand control screens. The control devices were treated as porous media, with an additional source term to model the pressure drop due the particle deposition. The results show the locations where the material depositions tend to occur and their influence on the increase of the pressure drop with the calcium carbonate incrustation. The increase on the pressure drop due the particles adhesion becomes more evident on higher Reynolds number. Future experiments will also permit to validate the numerical model and assist to improve the model as well.*

Keywords: *calcium carbonate deposition, computational fluid dynamics, completion engineering.*

1. INTRODUCTION

Due to the increase of the energetic demand, new technologies has been developed in order to promote the safety of oil extraction in petroleum reservoirs. The control of sand and particulates in oil wells is an indispensable completion technique. It occurs due to the complexity inherent to the exploration of offshore production wells, usually horizontal, where unconsolidated rock formations are found, such as friable sandstone reservoirs (Magalhães; Calderon; Martins, 2006).

Among the sand control techniques, the stand-alone screen stands out for its simplicity of installation and due to its effectiveness to retrain solids from the formation, with moderately selected grain size (Pessoa, 2011). In addition, the stand-alone screen configuration constitutes a lower cost alternative when compared to other sand control techniques.

The stand-alone screen technique configuration constitutes a perforated steel-based tube, wrapped by layers of screens that have the function of restraining the solids of the formation (Santos, 2007). There are also external layers that mechanically protect the filtration screens against abrasion and deformation.

During the secondary recovery process, the formation water, which contains lots of diluted minerals, in contact with the injected water can precipitate inorganic salts (Reis et al., 2011). One of the most common salts is the calcium carbonate, found in carbonated reservoirs. The calcium carbonate precipitation occurs according the chemical reaction:

$$Ca^{2+}{}_{(aq)} + 2HCO_{3\,(aq)}^{-} \leftrightarrow CaCO_{3(s)} + H_2O_{(l)} + CO_{2(aq)} \cdot \tag{1}$$

The salt crystals are normally carried with the flow, and can reach the sand control screens or the control valves. The salt can deposit in various regions of the well, including valves, sand control screens and on the reservoir regions near the well (Cosmo, 2013).

The deposition of the material, in a more critical context, can act to reduce the flow area, increasing the pressure drop, or completely obstruct the fluid passage. There is also the possibility of hindering or blocking the mechanical operation of certain completion elements (Maciel et al., 2019).

This study modelled the influence of the calcium carbonate deposition impact, assuming correlations present in the literature, for instance, Ergun (1952) equation, in order to evaluate the impact of the salt depositions on the pressure drop and fluid dynamics behaviour in sand control devices.

2. METHODOLOGY

2.1 Continuous phase flow

To model the fluid phase is necessary to determinate the flow regime. The Reynolds number is the relation between the inertial and viscous forces, used to verify the flow regime (Reynolds, 1889), calculated by:

$$\mathrm{Re} = \frac{8\rho\overline{u}^2}{\tau_w}, \tag{2}$$

where ρ is the fluid density, $\overline{u}$ is the characteristic velocity and τ_w is the wall shear stress, which for a pipe flow, can be calculated by:

$$\tau_w = \frac{8\mu\overline{u}}{D} \cdot \tag{3}$$

μ is the dynamic viscosity and *D* is the inlet pipe diameter. In the present study, the Reynolds number range from 1676 to 10057. Therefore, the flow regime was turbulent, transitional and laminar flow.

The condition of the continuous phase flow through the computational domain was assumed as isothermal, turbulent (except the lower Reynolds number evaluated, *Re* = 1676) and steady state flow to the fluid phase. The single-phase steady state flow was considered as the initial condition to the transient simulation of the multiphase flow, where the particles movement was tracked along the domain. The turbulence model *k–ε* is the simplest model for turbulence analyses and was used to model the turbulence on this study to reduce the computational cost, although the limitations.

2.2 Discrete phase modelling

The calcium carbonate ($CaCO_3$) particles were modelled as a dispersed solid represented by the Lagrange method, using the discrete phase model (*DPM*). This model can represent diluted systems with solid volume fraction lower than 10% (Maciel et al., 2019).

The solution of the velocity and particles position field of the discrete phase are individually solved, with the particle track equation, expressed by:

$$\frac{d\vec{u}_p}{dt} = F_d(\vec{v} - \vec{u}_p) - \vec{g}\frac{(\rho_p - \rho)}{\rho} + \vec{F}, \tag{4}$$

where $\vec{u}_p$ is the particle velocity, $\vec{v}$ is the eulerian phase velocity, ρ_p is the particle density, F represent the body forces (if any) and F_d is the drag force, calculate by:

$$F_d = \frac{18\mu}{\rho_p d_p^{\,2}} \frac{C_D \,\mathrm{Re}_p}{24}. \tag{5}$$

d_p is the particle diameter and Re_p is the relative Reynolds number between the continuous and discrete phase, calculate by:

$$\mathrm{Re}_p = \frac{\rho d_p \left| u_p - v \right|}{\mu}. \tag{6}$$

In order to model the particles of $CaCO_3$ with more accurately, it was considered a particle distribution, based on the calcium carbonate distribution obtained by the reaction presented on Eq. 1. Figure 1 shows the particle distribution used on the numerical simulation.

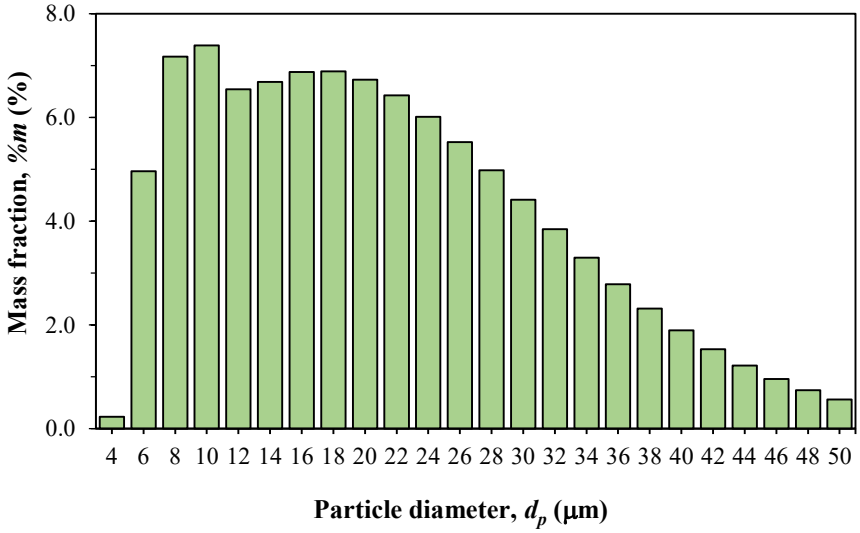

Figure 1. Calcium carbonate particle distribution used to perform the numerical simulations.

2.3 Geometry and mesh

The computational domain consist of a pipe, with a mechanical coupling, where the sand control screen and the support was connected. The pipe has 21 mm diameter. The pipe lengths, downstream and upstream for the mechanical coupling, were 50 mm and 100mm respectively. More details of the numerical geometry are show on Fig. 2.

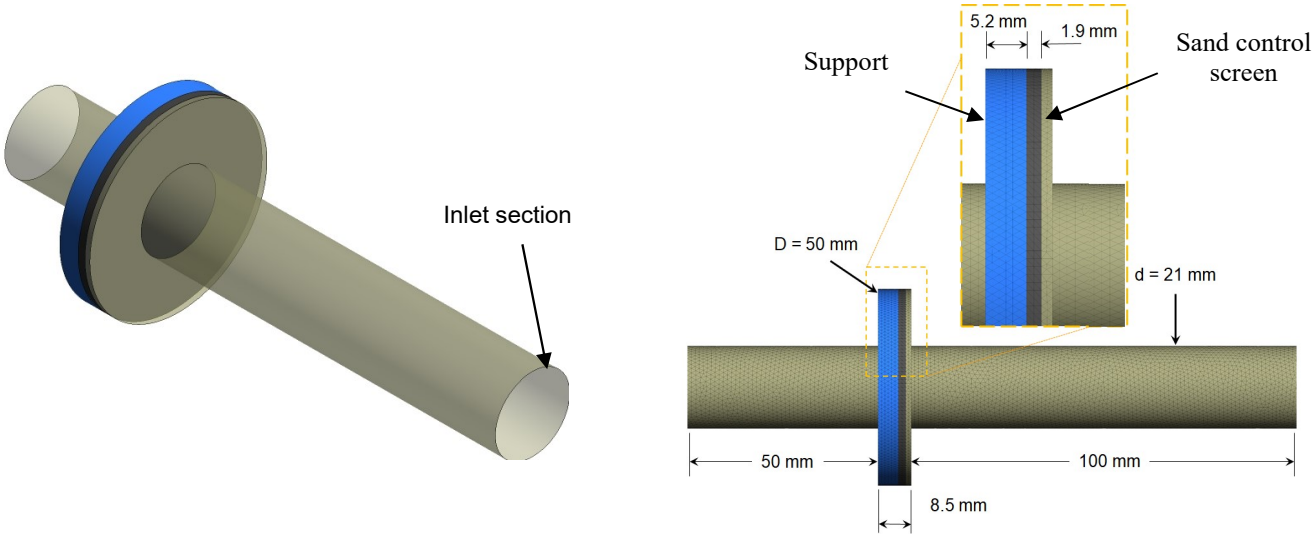

Figure 2. Schematic view of the computational geometry.

The computational discretization consist on a non-structured mesh, with 400,000 elements. The mesh was greeted using the standard parameter of the Ansys Meshing©, with a maximum element size of 1 mm and a refinement on the pipe section near the wall, with 4 elements, 1.2 growth rate and 0.25 mm of first layer height. Figure 3 show more details about the mesh.

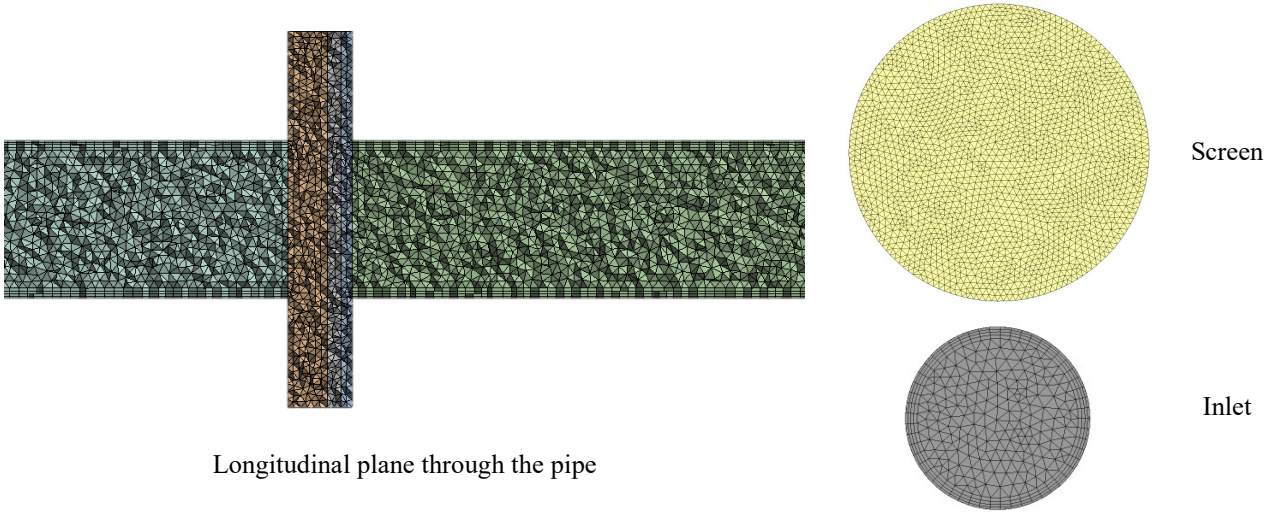

Figure 3. Computational mesh details.

The mesh have a maximum and minimum orthogonal quality of 1.0 and 0.22, respectively, and a maximum aspect ratio of 23.63.

2.4 Boudanry conditions

The flow rate range from 100 to 600 L/h, with a step of 100 L/h, using water as injected fluid, with density ρ = 998.2 kg/m³ and dynamic viscosity μ = 0.001003 Pa.s. The velocity profile at the inlet was considered as the fully developed turbulent profile. The outlet section was considered with atmospheric pressure (relative pressure of 0 Pa) and the walls with no slip condition.

The sand control devices was modelled using the Porous Media model. This model uses the Darcy-Forchheimer equation as a source term to increase the pressure drop on the domain, as expressed by:

$$S_\phi = -\left(\frac{\mu}{k^*} \vec{v}_f + C_2^* \frac{1}{2} \rho |v_f| \vec{v}_f \right), \tag{7}$$

where $1/k^*$ and C_2^* are the viscous resistance and inertial coefficient, respectively. To describe the incrustation effects on pressure drop, a user define function (UDF) was implemented, in order capture the particles of calcium carbonate and transform them on a physical coefficient, based on the Ergun (1952) equation. The correlation was adapted to model the changes of the coefficients as a function of the particles mass trapped on the cells domain, where the viscous resistance as a function of the particle mass concentration is:

$$\frac{1}{k^*} = A\left(1 - \frac{c}{\rho\phi_0}\right)^{-3} \left(\frac{1-\phi_0}{1-\phi_0+\frac{c}{\rho}} \right)^{-2}. \tag{8}$$

A is the initial viscous resistance of the screen, c is the particle mass concentration (kg/m^3) and ϕ_0 is the "porosity" of the screen. The inertial coefficient formulation is:

$$C_2^* = B\left(\frac{\phi_0}{\phi_0 - \frac{c}{\rho}} \right)^3 \left[1 + \frac{c}{\rho(1-\phi_0)} \right]. \tag{9}$$

B is the initial inertial coefficient of the screen. The constants *A* and *B* on Eq. 8 and 9 are 4.0 $x10^8$ $1/m^2$ and 28,250 $1/m$, respectively. The calcium carbonate particles, with density ρ_p = 2710 kg/m³, was injected with a mass flow rate m_p = 1.374 $.10^{-5}$ kg/s. When the particles collide with the screen, the macro *DEFINE_DPM_BC* activate, reading the particles properties and, if satisfied the adhesion criteria, calculate the mass concentration in the cell that the particle adhesion occurs.

Subsequently, the macro *DEFINE_PROPERTY* calculate the new constants of Eq. 7, and then the new fluid flow field is calculate. Figure 4 shows the flowchart of the simulation solver process.

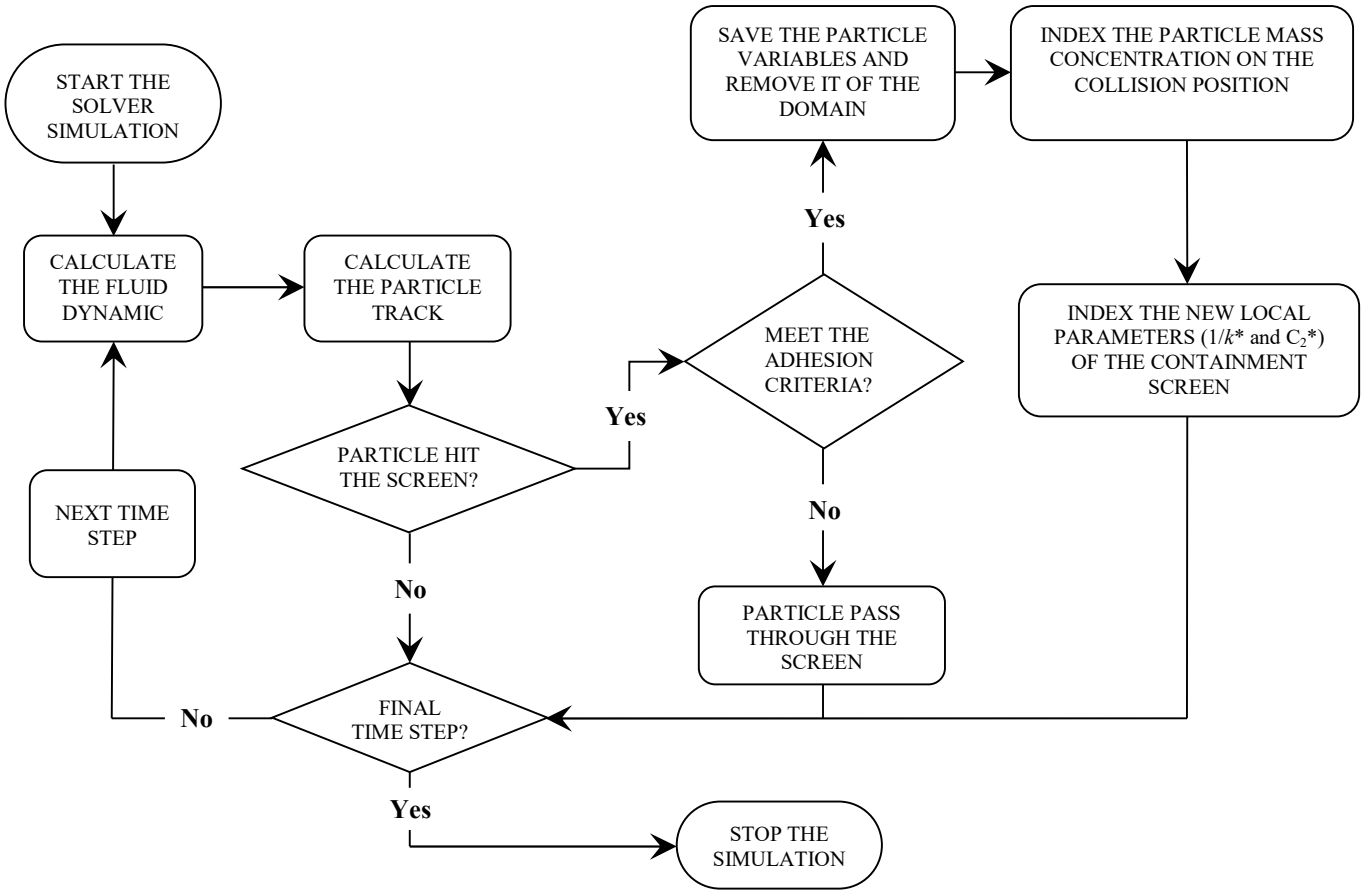

Figure 4. Simulation solver process with the UDF flowchart.

For each time step, the flowchart shown on Fig. 4 is executed. The simulations were performed up to 20s, with a time step of 0.001s and the adhesion criteria used it was, for instance, particle size larger than 10 μm.

3. RESULTS AND DISCUSSIONS

After the end of the solver process, the post processing of the simulation results was performed. The objective was verify the behaviour of the UDF to subsequent applications.

The adaptive properties of the screen with the particle adhesion permit to evaluate the incrustation pattern with the different flow rates evaluated and also permit to verify the influence of the $CaCO_3$ incrustation impact on the flow pattern (as the velocity profile across the containment screen and the changes on pressure drop).

The comparison of the $CaCO_3$ particle mass concentration on the containment screen to different Reynolds numbers after 20s of simulation are show on Fig 5.

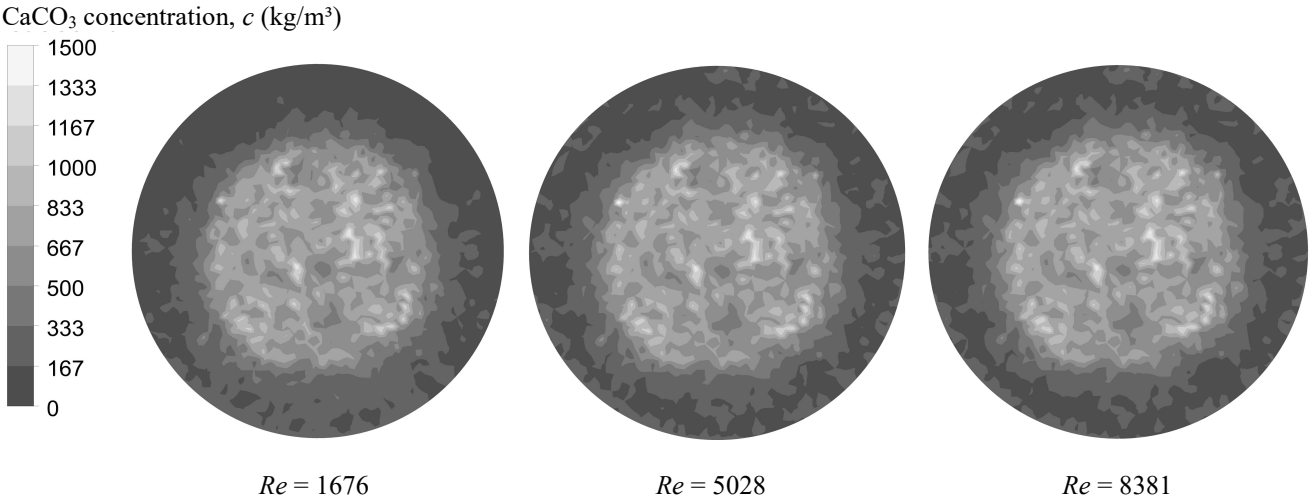

Figure 5. Influence of Reynolds number on the $CaCO_3$ mass concentration on the containment screen.

As shown in Figure 5, due the diameter of the inlet section being smaller than the screen diameter, the incrustation tends to occur preferentially on the center of the screen. It was also noted that there it is not a big difference between the adhesion pattern on the transitional and turbulent flow, but on the laminar regime is possible to see a little difference, due the low inertial forces, the gravitational forces make the particles deposit preferentially on the center and bottom section of the screen.

The small particles that are resulting of the $CaCO_3$ precipitation have low mass, and due to that, tends to be carry with the flow, and the gravitational effects can be noted only in laminar flow, as show Fig 5. One possible way to check the gravitational effects on the particles can be to increase the inlet section pipe, increasing the particle residence time and being able to verify the gravitational effects. Figure 6 shows the pressure drop as a function of time to different Reynolds number.

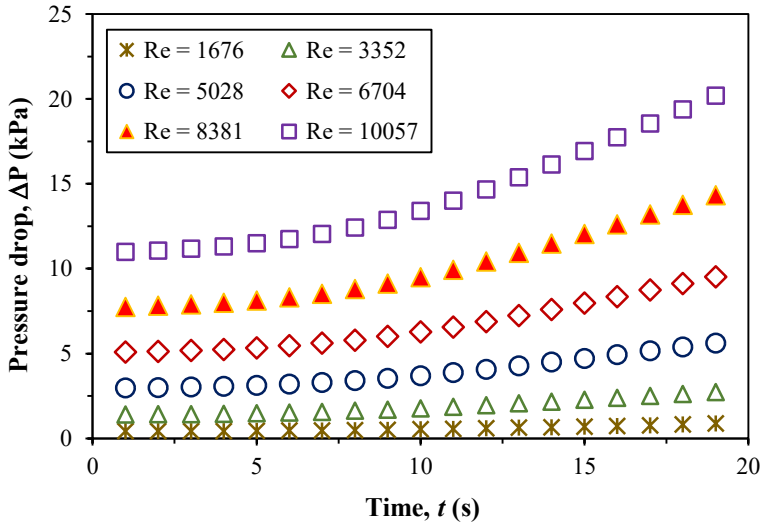

Figure 6. Influence of the particle adhesion on pressure drop.

Figure 6 shows that, using the approximation of the Ergun (1952) model, the influence of the incrustation on pressure drop becomes more evident at higher Reynolds number. On the beginning of the incrustation, the pressure drop increase slowly. This behaviour occurs because when the resistance at the center location of the screen increase, the flow tends to redistribute on the screen section. However, when the particle mass increase, there are no more changes on the flow pattern, but the resistance continue to increase while the particle deposited, making the pressure drop increase more drastically.

This behaviour becomes more evident when the velocity profile of the fluid phase is evaluated, as show Fig. 7.

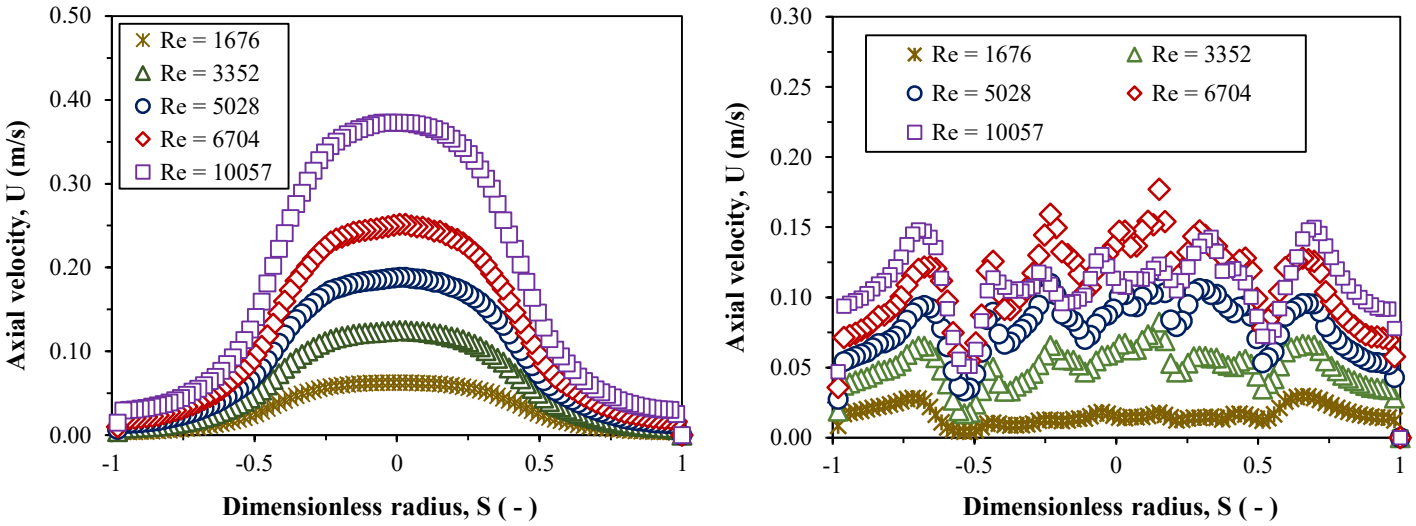

[a] t = 0s **[b]** t = 20s

Figure 7. Velocity profile on the sand screen (a) on the beginning of the simulation and (b) after 20s simulation.

As show Fig. 7 [a], without the $CaCO_3$ particles adhered on the sand screen, the higher velocity occurs on the center of the screen, especially due the pipe inlet section. With the incrustation of the particles (Fig. 7 [b]) and the increase of the resistance on center region of the sand screen, the flow tends to redistribute on the section of the screen.

It is possible to see on Fig 7 that to Reynolds number higher than 5000 without particles adhered the higher velocity increase, but with the particle adhesion, the fluid velocity on the center region it is almost the same, redirecting the flow to the sections neared to the wall.

4. CONCLUSION

This study shows an alternative method to simulate the calcium carbonate incrustation impact using correlations available on the literature to evaluate the influence of the particles deposition on the pressure drop in sand control screens. It was verified that the model was able to model the changes on the flow resistance due the presence of the $CaCO_3$ particles, as shown by the changes on the pressure drop and on the velocity profile on the sand screen. Performing an experimental investigation of the calcium carbonate particle incrustation is a way to verify the accuracy of the implemented model and implement the improvements necessary to the model. Finally, with the future realization of experiments, it will be also possible to validate the numerical model and assist the improvement of the model.

5. ACKNOWLEDGEMENTS

The authors would like to thank PETROBRAS for the financial support to carry this research and the Instituto Federal do Espírito Santo (IFES) and Universidade Federal do Espírito Santo (UFES) for the structure to develop this research.

6. REFERENCES

Cosmo, R. P. *Modelagem e simulação termodinâmica da precipitação de calcita em condições de poço*. 2013. 217 f. Dissertação (Mestrado) - Curso de Energia, Programa de Pós-graduação em Energia, Universidade Federal do Espírito Santo, São Mateus – ES, 2013.

Ergun, S. *Fluid Flow through Packed Columns*. Chemical Engineering Progress. Vol. 48, n. 2, p. 89-94, 1952.

Maciel, R. S.; Pereira, F. A. R.; Ribeiro, D. C. R. Martins, A. L.; Ferreira, M. V. D., 2019. "Modelagem da incrustação de cristais de carbonato de cálcio nas superfícies internas de válvulas de completação pela técnica de CFD". *Encontro Nacional de Construção de Poços de Petróleo e Gás – ENAHPE 2019*. Serra Negra, Brazil.

Magalhães, J. V.; Calderon, A.; Martins, A. L. Gravel Pack placement limits in extended horizontal offshore wells. *SPE Drilling & Completion*, [S.l.], v. 21, n. 03, p. 193-199, 1 set. 2006. Society of Petroleum Engineers (SPE).

Pessoa, T. F. P. *Análise Numérica de Medidas de Contenção de Sólidos em Rochas Produtoras de Óleo do Brasil*. 2011. 142 f. Dissertação (Mestrado) - Curso de Engenharia Civil, Programa de Pós-Graduação em Engenharia Civil da PUC-Rio, Pontifícia Universidade Católica do Rio de Janeiro, Rio de Janeiro, 2011.

Reis, M. I. P.; Silva, F. C.; Romeiro, G. A.; Rocha, A. A.; Ferreira, V. F. Mineral scale deposition in surfaces: problems and opportunities in the oil industry.: Problems and opportunities in the oil industry. *Revista Virtual de Química*, [S.l.], v. 3, n. 1, p. 2-13, 5 abr. 2011. Sociedade Brasileira de Química (SBQ).

Reynolds, O., 1883, An experimental investigation of the circumstances which determine whether the motion of water shall be direct or sinuous, and of the law of resistance in parallel channels. *Proceedings of the royal society of London*, Vol. 35, no. 224-226, p. 84-99.

Santos, A. R. *Análise do Colapso de Telas Utilizadas em Sistemas de Contenção de Areia em Poços Horizontais*. 2007. 123 f. Dissertação (Mestrado) - Curso de Engenharia Mecânica, Programa de Pós-graduação em Engenharia Mecânica, Pontifícia Universidade Católica do Rio de Janeiro, Rio de Janeiro, 2007.

7. RESPONSIBILITY NOTICE

The authors are the only responsible for the printed material included in this paper.